Energy Conversion and Management 250 (2021) 114858

Contents lists available at ScienceDirect

Energy Conversion and Management

journal homepage: www.elsevier.com/locate/enconman

Performance evaluation and improvement of thermoelectric generators (TEG): Fin installation and compromise optimization

Wei-Hsin Chen [a,b,c,*], Chi-Ming Wang [a], Lip Huat Saw [d], Anh Tuan Hoang [e], Argel A. Bandala [f]

[a] Department of Aeronautics and Astronautics, National Cheng Kung University, Tainan 701, Taiwan
[b] Research Center for Smart Sustainable Circular Economy, Tunghai University, Taichung 407, Taiwan
[c] Department of Mechanical Engineering, National Chin-Yi University of Technology, Taichung 411, Taiwan
[d] Lee Kong Chian Faculty of Engineering and Science, Tunku Abdul Rahman University,Kajang 43000, Malaysia
[e] Institute of Engineering, Ho Chi Minh City University of Technology (HUTECH), Ho Chi Minh City, Viet Nam
[f] Department of Electronics and Communications Engineering, De La Salle University, 2401 Taft Avenue, Manila 0922, The Philippines

ARTICLE INFO

Keywords:
Thermoelectric generator
Plate and square pin fins
Waste heat recovery
Source term
Computational fluid dynamic
Compromise method

ABSTRACT

How to improve the performance of thermoelectric generators is an important issue to recover waste heat and convert it into green power, which is conducive to practicing net-zero carbon dioxide emissions. The heat transfer and power generation of a thermoelectric module (TEM) under the influence of fin installation is investigated by three-dimensional fully numerical simulations where vehicle exhaust waste heat is harvested. This study considers a TEM in a hot channel without fins as well as with plate fins and square pin fins, while a cold channel is used to cool the TEM. The results show that installing plate fins or square pin fins can drastically intensify waste heat harvest, and the optimal number of square pin fins is 78 which increases the output power of the TEM by 24.14% compared to the plate fins. A compromise method in terms of heat flow rate ratio and heat flow rate ratio per unit area of square pin fins is conducted, which simultaneously considers the TEM's output power and material cost. As a result, it is found that the optimal number of square pin fins is 54. The influences of the temperature and mass flow rate of the hot fluid on TEM performance are also evaluated, and the results indicate that the former has a pronounced impact whereas the latter is relatively unimportant. Installing more square pin fins gives rise to a higher pressure drop. Nevertheless, the net output power of the TEM increases with increasing the number of square pin fins and the highest value occurs at 78.

1. Introduction

With the development of industrialization, a large amount of industrial waste heat has posed serious environmental problems such as global warming and deteriorated atmospheric greenhouse gas emissions [1]. In recent years, converting thermal energy from waste heat into electrical energy has attracted a great deal of interest [2]. The phenomenon of thermoelectricity (TE) was discovered in the 18th century. The TE theory is mainly based on the Seebeck effect (mainly thermoelectric generators or TEGs) and the Peltier effect (mainly thermoelectric coolers or TECs) [3]. The advantages of TEGs include no moving parts or refrigerants, no chemical reactions and gas emissions, long service life, being environmental-friendly, flexible operation, etc [4]. They can be used in a wide range of fields such as vehicle exhaust pipes [5], steel and petrochemical industries, solar energy [6], and hot springs.

To effectively harvest the waste heat emitted in the industry and increase the performance of the TE system, in addition to changing the thermoelectric material [7], it is also an efficient countermeasure to insert fins into hot channels [8]. Fins can increase the heat transfer area [9] and increase the temperature of the hot side of the thermoelectric module (TEM) to obtain higher output power. The types of fins can be divided into cylindrical pin fins [10], square pin fins [11], plate fins, and others [12]. But the accompanying disadvantage of installing fins is that the pressure drop will increase. Square pin fins can achieve a greater heat transfer area in a lower volume compared to plate fins, making their heat transfer efficiencies higher than the plate-fins. Moreover, the thermal resistance of pin-fins is lower than that of plate-fins. In other words, the pin fins can lower the required material cost while improving heat transfer performance [13].

Considering the applications of fin, Jonsson et al. [14] studied seven

* Corresponding author.
E-mail addresses: weihsinchen@gmail.com, chenwh@mail.ncku.edu.tw (W.-H. Chen).

https://doi.org/10.1016/j.enconman.2021.114858
Received 30 June 2021; Received in revised form 25 August 2021; Accepted 8 October 2021
Available online 22 October 2021

Nomenclature

A	Surface area (mm^2)
a	Coefficient
b	Contribution of the source term
C	Specific heat capacity (J)
$C_{1\varepsilon}, C_{2\varepsilon}, C_{3\varepsilon}, C_\mu$	Constant
$\dot{E}$	Energy per unit volume ($W{\cdot}m^{-3}$)
$\vec{E}$	Electric field intensity vector ($V{\cdot}m^{-1}$)
$\dot{g}$	Power generation per unit volume ($W{\cdot}m^{-3}$)
I	Electric current (A)
k	Thermal conductivity ($W{\cdot}m^{-1}{\cdot}K^{-1}$)
$\dot{m}$	Mass flow rate ($kg{\cdot}s^{-1}$)
P_{out}	Output power (W)
P	Pressure (W)
ΔP	Pressure drop (Pa)
Q	Heat flow rate (W)
Q_r	Heat transfer rate ratio
Q_s	Heat flux ratio
$\dot{q}$	Heat flux ($W{\cdot}m^{-2}$)
$\vec{q}$	Heat flux vector ($W{\cdot}m^{-2}$)
R	Universal gas constant (=8.314 $m^3{\cdot}Pa\ K^{-1}{\cdot}mol^{-1}$)
R_{TE}	Electric resistance (Ω)
$R_{external}$	External load resistance (Ω)
S	Seebeck coefficient ($V{\cdot}K^{-1}$)
S_g	Source term in energy equation ($W{\cdot}m^{-3}$)
T	Temperature (K)
V	Velocity ($m{\cdot}s^{-1}$)
$\forall$	Volume (m^3)
x, y, z	Cartesian coordinates

Greek letters

η	Efficiency (%)
μ	Dynamic viscosity (Pa·s)
μ_t	Turbulent (or eddy) viscosity
ρ	Density ($kg{\cdot}m^{-3}$)
ρ_e	Electrical resistivity (Ω·m)
σ_k	Turbulent Prandtl numbers for k
σ_ε	Turbulent Prandtl numbers for ε
$\varnothing$	General variable

Subscripts

ave	average
c	Cold side of TE element
h	Hot side of TE element
n	*n*-type TE element
p	p-type TE element
st	Storage
TE	Thermoelectric element
th	Thickness of the TEM

different geometries of heat sinks and considered the effects of duct height, duct width, fin height, fin thickness, and interval of fin-to-fin. Jang et al. [15] studied the influence of the flow channel with plate-fins on the output power and pressure drop of the TEM system by changing the height and number of the fins at different inlet velocities and temperatures. Rezania et al. [16] studied the net output power of a TEM with plate fins and cross-cut fins at different inlet velocities and found the maximum net output power of the TEM within the investigated inlet velocities. Şara [17] studied the heat transfer performance of square pin-fins in a rectangular flow channel, analyzed the effects of the fin gap and fin height to the gap ratio between the fin and the channel on the performance of the heat exchangers, and adopted a staggered arrangement to improve heat transfer. Peltonen et al. [18] studied the local heat transfer in a flow channel with plate fins and square pin fins. The results showed that local vortices were generated when the fluid flowed through the array of square pin fins, which doubled the local heat transfer. Yang et al. [19] carried out a comparison of the performances of the square, cylinder, and elliptical pin fins. From their results, it was found that the heat transfer coefficients of the pin fins were much higher than that of the plate-fins. When the square and cylinder pin fins were arranged in a line and the number was equivalent, the heat transfer coefficient of the square pin fins was higher than that of the cylinder pin fins, and the heat transfer coefficients increased as the density of the fins increased.

To obtain the temperature at the hot side and cold side of a TEG and the pressure drop in the flow channel, the TEG can be combined with computational fluid dynamics (CFD) to build a three-dimensional model and predict and optimize the performance of the thermoelectric system. Chen et al. [20] established a three-dimensional model to observe the temperature distribution and current generated from thermoelectric generators by CFD. Seo et al. [21] studied the performance of a TEM in a flow channel with plate-fins, and observed the influences of fin parameters on the TEM through CFD, and compared it with experimental data. Bejjam et al. [22] studied the effect of changing the material of the heat exchanger and the outlet gap on the performance of thermoelectric generators through CFD for three-dimensional modeling and heat transfer analysis at the hot and cold inlet temperatures of 800 K and 350 K, respectively. Luo et al. [23] proposed a multi-physical coupling numerical model of transient CFD and thermal electric field to explore the performance of automotive thermoelectric generator systems and compare the output power of the steady-state numerical simulation and the transient numerical simulation for proposing a better model to evaluate the automobile thermoelectric generator system. Based on these studies, it is known that CFD is an efficient and reliable tool to predict the performance of thermoelectric generator systems.

Among different types of fins, plate fins and square pin fins are suitable for recovering industrial low-temperature waste heat since they have good heat transfer performance and lower materials cost. To predict the output power and pressure drop characteristics of the thermoelectric system, this research aims to establish a three-dimensional model by combining CFD with a TEM to simulate and optimize the performance of the system. The review of past literature suggests that few studies compared the heat transfer performance of square pin fins and plate-fins in thermoelectric systems. Therefore, this research embeds plate fins and square pin fins in a hot channel to increase the waste heat harvest at the hot side of a TEM, and compares the output power and conversion efficiency of the TEM with plate fins and different numbers of square fins. A comparison between the results without fins as well as with plate fins and square pin fins is also carried out. The changes in mass flow rates and hot fluid temperatures are also considered to explore their influences on the TEM's performance. At last, the most suitable geometric size and operating conditions at different hot inlet temperatures and mass flow rates are suggested.

2. Methodology

2.1. Physical configuration

In this study, two different types of fins are inserted into the hot channel, so the average temperature difference between the hot side and cold side of the TEM is intensified to trigger and enhance the Seebeck effect, thereby generating power. The physical configuration of this study includes a hot channel with a hot flue gas, a cold channel with cold water, and a thermoelectric module, as shown in Fig. 1. The hot and cold channels are rectangular, and their sizes are identical with length × width × height = 200 mm × 84 mm × 54 mm. The thickness of the rectangular channel is 2 mm. The TEM uses a commercial thermoelectric module (TEC1-12706) [20], which is mainly composed of 127 pairs of p-type and *n*-type semiconductors. The semiconductor's material is Bi_2Te_3, and the leg's size is 40 mm × 40 mm × 3.75 mm (length × width × height). The TEM is located between the hot and cold channels. To save the calculation time, the TEM's properties are assumed to be a constant [24]. The detailed thermoelectric properties, waste heat flue gas, and cooling water parameters are listed in Table 2.

To increase the TEM's hot side average temperature, two types of fins, namely, plate fins and square pin fins are employed. Both of them are made of aluminum, as shown in Table 2. There are 6 plate fins (Fig. 2**a**) with an individual dimension of 40 mm × 2.5 mm × 30 mm (length × width × height). The preliminary geometry of the pin fins is designed based on the literature. Kim et al. [25] mentioned that when the fin's thickness was 2.5 mm, it could be applied to a wide range of applications. For this reason, the square pin fin's size is 2.5 mm × 2.5 mm × 30 mm (length × width × height), and the configurations of the square pin fins are arranged from 6 × 6 (row × column) to 14 × 6, implying that the number of square pin fins is from 36 to 84 (Fig. 2**b-2 k)**. The determination of the optimal number of fins depends on the output power produced by the TEM and pressure drop. After evaluating the two physical quantities, the most suitable find configuration can be attained for waste heat recovery.

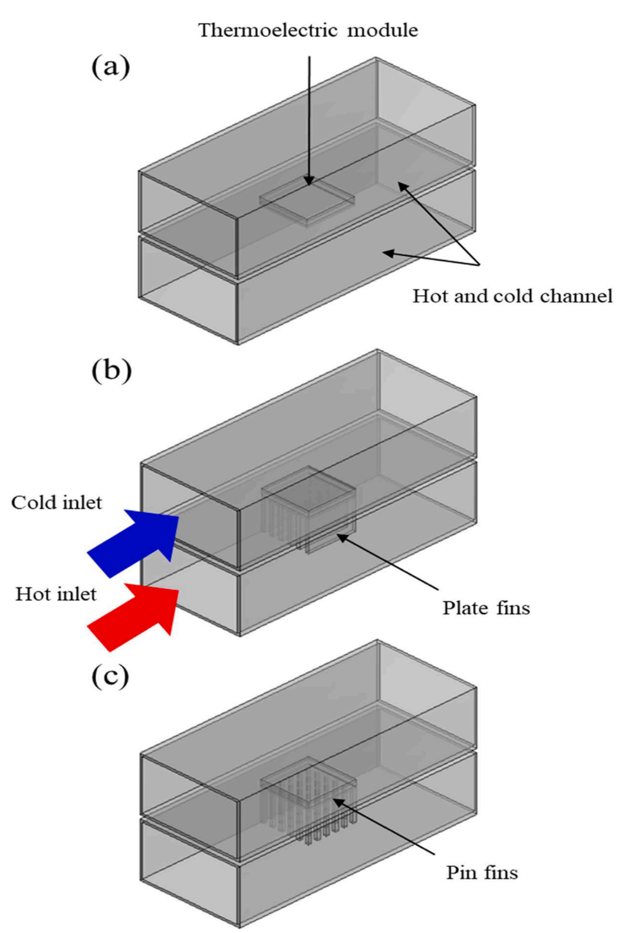

Fig. 1. Physical model of (a) without fin (b) plate fins (c) square pin fins.

2.2. Mathematical formulations

2.2.1. Governing equations of turbulence flow

In this study, the fluid is assumed to be of incompressible flow, and the fluid properties are assumed to be constant. The flows are three-dimensional turbulent and steady inasmuch as the Reynolds numbers of hot and cold fluids are 15,115–26,991 and 7,655, respectively. The effect of heat radiation is ignored. The commercial software ANSYS Fluent 2019 *R*3 is used to calculate the flow field, heat transfer, and pressure drop characteristics of the channels. The standard k-ε model is suitable for fully turbulence flow with high Reynolds numbers [26] and is thus adopted in the CFD simulation to observe the flow fields and pressure drops in the channels. The relevant governing equations as well as turbulent kinetic energy (k) and dissipation rate (ε) are given as follows.

Continuity equation

$$\nabla\bullet\left(\rho\vec{\mathrm{V}}\right)=0 \tag{1}$$

Momentum equation

$$\rho\vec{V}\bullet\nabla\vec{\mathrm{V}}=-\nabla\mathrm{P}+\nabla\bullet\left[\mu\left(\nabla\vec{\mathrm{V}}+\left(\nabla\vec{\mathrm{V}}\right)^{\mathrm{T}}\right)\right] \tag{2}$$

Energy equation

$$\nabla\bullet\left(\vec{\mathrm{V}}\rho\mathrm{C_p}\mathrm{T}\right)=\nabla\bullet(\mathrm{k}\nabla\mathrm{T})+\mathrm{S_g} \tag{3}$$

Turbulence kinetic energy, k

$$\frac{\partial}{\partial x_i}(\rho k u_i)=\frac{\partial}{\partial x_j}\left[\left(\mu+\frac{\mu_t}{\sigma_k}\right)\frac{\partial k}{\partial x_j}\right]+G_k+G_b-\rho\varepsilon-YM+S_k \tag{4}$$

Dissipation rate, ε

$$\frac{\partial}{\partial x_i}(\rho\varepsilon u_i)=\frac{\partial}{\partial x_j}\left[\left(\mu+\frac{\mu_t}{\sigma_\varepsilon}\right)\frac{\partial\varepsilon}{\partial x_j}\right]+C_{1\varepsilon}\frac{\varepsilon}{k}(G_k+C_{3\varepsilon}G_b)-C_{2\varepsilon}\rho\frac{\varepsilon^2}{k}+S_\varepsilon \tag{5}$$

where G_k and G_b denotes the generation of turbulence kinetic energy due to shear and buoyancy, and $\mu_t=\rho C_\mu\frac{k^2}{\varepsilon}$, $C_{1\varepsilon}=1.44$, $C_{2\varepsilon}=1.92$, $C_\mu=0.09$, $\sigma_k=1.0$, and $\sigma_\varepsilon=1.3$. The above constants have been determined in basic turbulence experiments [27].

2.2.2. Thermoelectric module (TEM)

In this study, the TEM is used to recover waste heat and the utilized waste heat that is discharged into the environment. In the calculation process, the heat equation in the control volume of TEM is determined through the first law of thermodynamics as follows:

$$\sum\dot{Q}_{in}-\sum\dot{W}_{out}+\dot{E}_g=\dot{E}_{st} \tag{6}$$

where $\dot{E}_g(=\dot{g}dxdydz)$ is the energy generation rate per unit volume of the TEM, $\dot{E}_{st}\left(=\rho_{TE}C\frac{\partial T}{\partial t}dxdydz\right)$ is the energy depository rate, respectively, and ρ_{TE} and C are the density and specific heat capacity of the thermoelectric materials, respectively. In the control volume, this study treats the TEM as a source term, and the heat transfer equation according to the first law of thermodynamics is given as follows:

$$(\dot{q}_x-\dot{q_{x+dx}})dydz+(\dot{q}_y-\dot{q_{y+dy}})dxdz+(\dot{q}_z-\dot{q_{z+dz}})dxdy+\dot{E}_g=\dot{E}_{st} \tag{7}$$

where $\dot{q}$ is the heat flux. $\dot{E}_g$, $\dot{E}_{st}$ and Fourier's law ($=-k\nabla T$) are substituted into Eq. (7). The heat equation is divided by volume ($dxdydz$) yields as follows:

$$\frac{\partial}{\partial x}\left(k\frac{\partial T}{\partial x}\right)+\frac{\partial}{\partial y}\left(k\frac{\partial T}{\partial y}\right)+\frac{\partial}{\partial z}\left(k\frac{\partial T}{\partial z}\right)+\dot{g}=0 \tag{8}$$

where k and $\dot{g}$ represent the thermal conductivity and source terms, respectively. The term $\dot{g}$ represents the power generation per unit

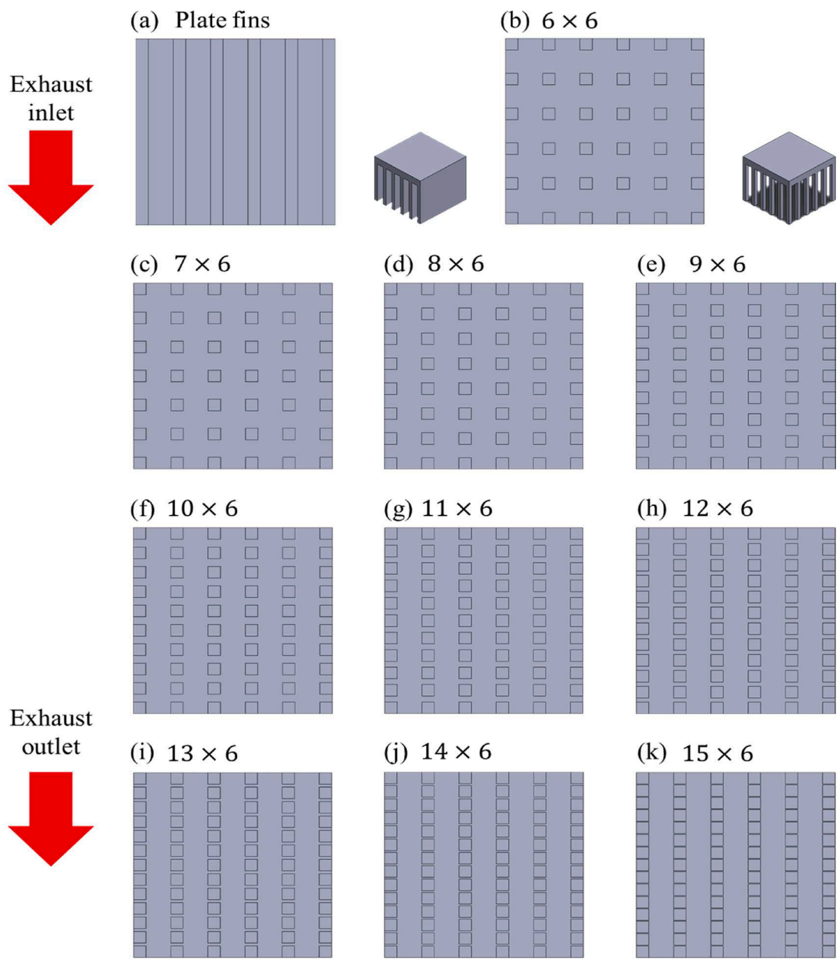

Fig. 2. The bottom of (a) plate fins and different numbers of (b-k) square pin fins.

volume from the self-consistency theory [28].

To simplify the time required for the simulation, this study postulates that the properties of the thermoelectric material are constant, and ignores the Thomson effect. Consequently, the average temperature difference between the hot and cold sides of the TEM causes a temperature gradient and then induces current as follows [29]:

$$I = \frac{S\Delta\overline{T}}{R_{TE} + R_{external}} \tag{9}$$

where S is the Seebeck coefficient of the TEM ($S = S_p - S_n$), R_{TE} is the internal resistance from TEM, and $R_{external}$ is the external load resistance. The output power produced by the TEM is [30]:

$$P_{out} = I^2 R_{external} = \left(\frac{S\Delta\overline{T}}{R_{TE} + R_{external}}\right)^2 R_{external} \tag{10}$$

To attain the maximum output power [31], this research considers the impedance matching of TEM, and the formula is given as:

$$R_{TE} = R_{external} \tag{11}$$

In other words, the external resistance is equal to the internal resistance of the TEM. From the impedance matching, the maximum output power can be fulfilled from Eq. (10), that is [32]:

$$Maximumpower = \frac{S^2\Delta\overline{T}^2}{4R} \tag{12}$$

Accordingly, the source term $\dot{g}$ ($= S_g$) is the maximum output power generated by the TEM per unit volume at a given temperature difference, and is shown as:

$$\dot{g} = -\frac{\frac{S^2\Delta\overline{T}^2}{4R}}{\forall} \tag{13}$$

where $\forall$ is the total volume of the TEM. Therefore, the source term $\dot{g}$ is negative. Substituting Eq. (13) into Eq. (8) along with the constant material properties yields:

$$\frac{\partial^2 T}{\partial x^2} + \frac{\partial^2 T}{\partial y^2} + \frac{\partial^2 T}{\partial z^2} - \left[\frac{\frac{S^2\Delta\overline{T}^2}{4R}}{\forall k}\right] = 0 \tag{14}$$

The average temperature difference between the hot and cold ends of the TEM can be obtained through the results of CFD, and the power generation of the TEM can be obtained through the average temperature difference. Seeing that the TEM's thickness is muck shorter than its length and width, it is feasible to postulate that heat is only transferred along x-dimension. So Eq. (14) becomes:

$$\frac{d^2 T}{dx^2} + \frac{\dot{g}}{k} = 0 \tag{15}$$

Double integration of Eq. (15) represents the TEM's temperature function as follows:

$$T(x) = -\frac{\dot{g}}{2k}x^2 + c_1 x + c_2 \tag{16}$$

The values of c_1 and c_2 can be obtained the average temperature of the hot side($x_{th,h} = 0$ mm) and cold side($x_{th,c} = 3.75$ mm). From Eq. (16), The heat fluxes from the waste heat channel through the hot side of the

TEM ($\dot{q}_H$) and lost from the cold side of the TEM to the cooling channel ($\dot{q}_L$) are written as

$$\dot{q}_H = -k_{TE}\frac{dT_H}{dx} \tag{17}$$

$$\dot{q}_L = -k_{TE}\frac{dT_L}{dx} \tag{18}$$

Accordingly, the output power of the TEM is $P = \left(\dot{q}_H - \dot{q}_L\right) \times A_{TEM}$. In thermoelectricity, the conversion efficiency of the TEM is an important indicator for converting thermal into electrical energy. The conversion efficiency η of the TEM is written as:

$$\eta(\%) = \frac{P}{Q_H} \times 100 = \frac{\dot{q}_H - \dot{q}_L}{\dot{q}_H} \times 100 \tag{19}$$

where Q_H is the waste heat flow rate to the TEM.

2.3. Numerical method and validation

2.3.1. Numerical method

To simulate the waste heat recovery of an automotive exhaust, this research uses the commercial package software ANSYS 2019 *R*3 to solve the aforementioned equations. In the pressure–velocity coupling solutions, the SIMPLEC algorithm is utilized, and the Least Squares Cell Based on the spatial discrete solution is selected. In the solving process, the residual sum is given as follows:

$$\text{Residual sum} = \sum_{\text{domain}} |a_{nb}\varnothing_{nb} + b - a_P\varnothing_P| \tag{20}$$

where a is coefficient, $\varnothing$ is generally variable, and$b$ is the contribution of the constant part of the source term [15]. When the sums of the residuals of continuity, energy, turbulent kinetic energy, and dissipation rate are all less than 10^{-6}, the calculation reaches convergence and the iteration is terminated.

The simulation procedure is described as follows. First, the mass flow rates and temperatures of the hot and cold fluids are set. From the governing equations (1) to (5), the temperature profiles and average temperatures at the hot-side and cold-side surfaces can be attained, which can further obtain the average temperature difference between the hot and cold sides of the TEM, and thereby the source term from Eq. (13). The source term is then substituted into Eq. (3) followed by iteratively solving Eqs. (1)-(5) until achieving the convergent criteria. Thereafter, one can acquire the temperature distribution in the TEM, the heat fluxes at the hot side and cold side, output power, and the efficiency from Eqs. (16)-(19). The detailed calculation process is shown in Fig. 3. Accordingly, thermoelectricity and CFD are combined to reduce the calculation time without losing accuracy.

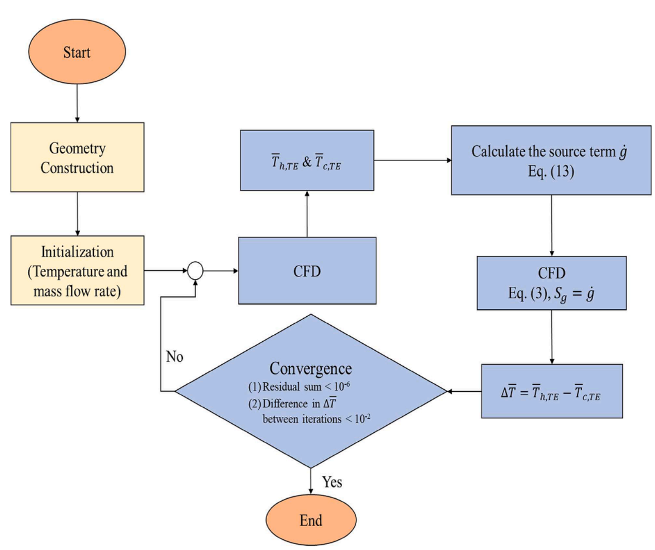

Fig. 3. The flowchart of the calculation process.

2.3.2. Validation of the turbulent model

Before performing predictions, this study compares the simulation results with experimental data to validate the accuracy of the results. The geometric dimensions and operating conditions are established based on the study of Selimefendigil et al. [33] where the flow was turbulence. The comparison between the numerically simulated and experimental Nusselt numbers under different Reynolds numbers is shown in Fig. 4 where the Reynolds number ranges from 6,529 to 32,646. The average relative error between the simulations and experimental data is less than 5 % whereby the numerical validity is ascertained.

2.3.3. Grid independence of the system and validation of the thermoelectric module

The confirmation of the grid independence of the simulation model is another essential task prior to predictions. This study includes three different configuration systems. The first system is the hot channel without fins, the second one is the hot channel with plate fins, and the third one is the hot channel with square pin fins (6 × 6). In the three systems, the following five different numbers of grids are individually established. Five different numbers of grids 87,093, 112,924, 271,460, 520,483 and 620,472 are calculated in the first system, five numbers of grids 97,289, 168,082, 314,826, 675,446 and 1,248,757 are considered in the second system, and also five numbers of grids 116,855, 223,337, 389,811, 676,399 and 1,216,279 are regarded in the last system. The results in Fig. 5 show that the profiles of the average temperature difference between the hot side and the cold side of the TEM at the three configuration systems under different numbers of grids. Based on the requirement of the relative error less than 1 % with increasing the mesh number to satisfy the grid independence, the grids of 271,460, 314,826, and 389,811 are adopted for simulation in the first, second, and third systems, as listed in Table 1. Moreover, the grid independence tests are also carried out at different numbers of square pin fins, and the suitable grid numbers are shown in Table 1 as well. The TEM used in this study (TEC1-12706) is the same as that in previous work [24] in which the rigorous validation has been fulfilled. Specifically, the maximum error compared with the experimental data was lower than 6 %.

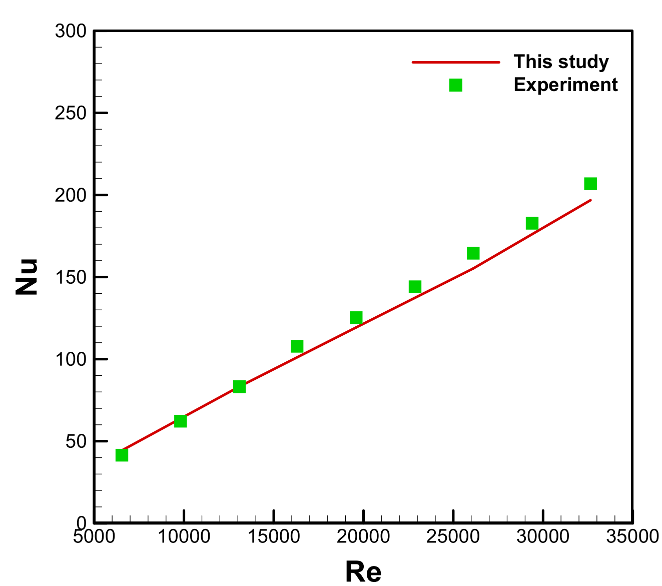

Fig. 4. Comparisons of Nusselt numbers between simulated and experimental data [33] under different Reynolds numbers.

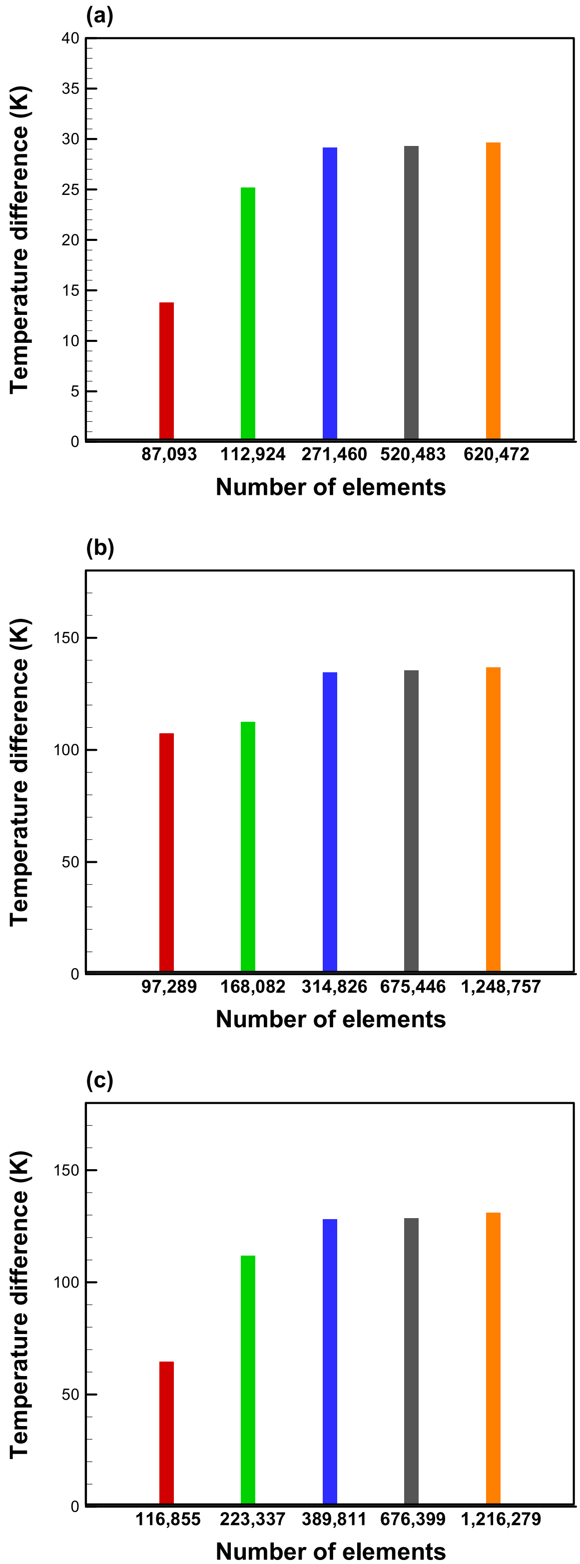

Fig. 5. Grid independent of (a) without fins (b) plate fins (c) square pin fins (36). ($\dot{m}_h = 0.028\text{kg}\bullet\text{s}^{-1}$ and $T_h = 603.15\text{K}$).

2.4. Operating and boundary conditions in the system

In this study, the hot fluid is the automotive exhaust, which is assumed to be turbulent, and the cold fluid is water in an industrial cooling system. The operating conditions include the mass flow rates and temperatures of the automotive exhaust where the properties of the fluids (i.e., hot exhaust and cooling water) are shown in Table 2 [34]. Automotive exhaust belongs to medium-temperature waste heat, and its temperature range is 230–650 °C [35]. In this study, the temperature of the waste heat flue gas is set to be 230–430 °C (=503.15–703.15 K). The cold fluid is water, and its mass flow rate and temperature are fixed at 0.5 kg·s^{-1} and 30 °C (=303.15 K) in this study. The outlets of the cold and hot fluids are assumed at atmospheric pressure (=1 atm). For the boundary conditions, the channel walls and the lateral surfaces of the TEM are adiabatic; nevertheless, the contact surfaces between the channels and the TEM have heat transfer, causing the temperature difference between the hot and cold sides of the TEM to generate electricity. When the fluids flow through the channels, the no-slip boundary condition is imposed on the channel walls. Detailed boundary conditions are sketched in Fig. 6.

Table 1
Grid independence of different numbers.

Configurations of square pin fins	Number of grids	Mesh elements
Without fin	271,460	Tetrahedral and hexahedron
Plate fins	314,826	Tetrahedral and hexahedron
Square pin fins		Tetrahedral and hexahedron
6 × 6	389,811	Tetrahedral and hexahedron
7 × 6	397,678	Tetrahedral and hexahedron
8 × 6	403,440	Tetrahedral and hexahedron
9 × 6	408,471	Tetrahedral and hexahedron
10 × 6	420,065	Tetrahedral and hexahedron
11 × 6	430,306	Tetrahedral and hexahedron
12 × 6	431,066	Tetrahedral and hexahedron
13 × 6	568,156	Tetrahedral and hexahedron
14 × 6	658,651	Tetrahedral and hexahedron
15 × 6	1,470,679	Tetrahedral and hexahedron

Table 2
Properties of the adopted TEM material, exhaust, and water.

Parameter	Unit	Value
TEM [20]		
Seebeck coefficient	$V{\cdot}K^{-1}$	$S_p = -S_n = 226.8 \times 10^{-6}$
Thermal conductivity	$W{\cdot}m^{-1}{\cdot}K^{-1}$	$k_p = k_n = 1.52$
Resistivity	$\Omega{\cdot}m$	$\rho_p = \rho_n = 1.447 \times 10^{-5}$
Hot flue gas [34]		
Density	$kg{\cdot}m^{-3}$	0.644
Specific heat at constant pressure	$J{\cdot}kg^{-1}{\cdot}K^{-1}$	1045
Thermal conductivity	$W{\cdot}m^{-1}{\cdot}K^{-1}$	0.0444
Viscosity	$kg{\cdot}m^{-1}{\cdot}s^{-1}$	2.85×10^{-5}
Cooling water		
Density	$kg{\cdot}m^{-3}$	998.2
Specific heat at constant pressure	$J{\cdot}kg^{-1}{\cdot}K^{-1}$	4182
Thermal conductivity	$W{\cdot}m^{-1}{\cdot}K^{-1}$	0.6
Viscosity	$kg{\cdot}m^{-1}{\cdot}s^{-1}$	0.001003
Aluminum		
Density	$kg{\cdot}m^{-3}$	2719
Specific heat	$J{\cdot}kg^{-1}{\cdot}K^{-1}$	871
Thermal conductivity	$W{\cdot}m^{-1}{\cdot}K^{-1}$	202.4

3. Results and discussion

3.1. Isothermal contours in the waste heat recovery system

3.1.1. Top surface of the hot channel

To understand the influences of installing fins on the temperature distribution of the hot side of the TEM, Fig. 7 shows the isothermal contours at the upper surface of the hot channel without fins, with plate fins, and with different numbers of square pin fins. The mass flow rate and temperature of the hot exhaust are 0.028 kg·s^{-1} and 603.15 K, respectively. It can be found that when the hot fluid flows through the TEM, its temperature drops dramatically, irrespective of which system is adopted. This is a consequence of waste heat absorbed by the TEM and transferred into the cold fluid. Accordingly, a temperature difference

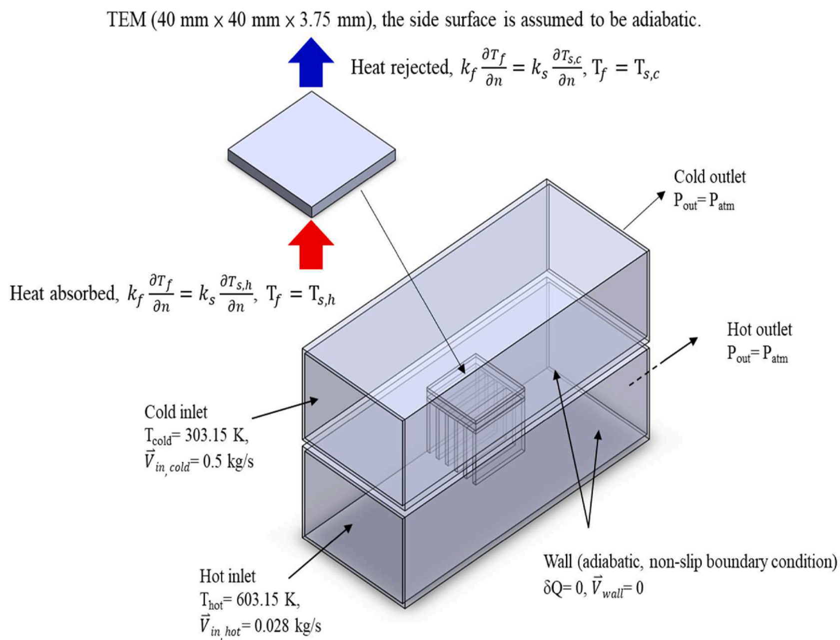

Fig. 6. Boundary conditions of (a) the hot and cold fluid, channel, and fins.

between the two sides of the TEM is induced to generate electricity and then achieve waste heat recovery [36–38]. In the system without fins (Fig. 7**a**), overall, the downstream temperature of the TEM is higher than those with plate (Fig. 7**b**) and square pin fins (Fig. 7**c-7 l**), showing the more efficient heat absorption by the fins. Kim et al. [25] studied the effect of different numbers of plate fins on the hot side temperature of a TEM and found that the temperature increased as the number of fins rose, and the maximum temperature increased from 375 K to 502 K. For the system with square pin fins, it is also observed that the isothermal contours in the intervals between the fins have a trend to increase. However, once the number of square pin fins increases to a certain extent, the isothermal contours in the interval are prone to decline. Specifically, once the number of square pin fins exceeds 78 (Fig. 7**j**), the interval temperatures are lower. This can be explained by the smaller average heat absorption amount by each fin, whereby the temperature gradients around the fins become smaller. Moreover, the intervals of the square pin fins are too small, and the hot fluid can't easily flow between the square pin fins. As a result, the temperature around the square pin fins becomes lower.

3.1.2. Plate and square pin fins

The isothermal contours of the hot plate under the TEM, the outermost plate fin, and the outermost square pin fins are demonstrated in Fig. 8**.** Fig. 8**a** shows the cross-sectional temperature distribution of the hot plate under the TEM without fins where it can be found that the temperature is much lower compared to other cases, stemming from no fins installed to absorb waste heat from hot fluid [39]. This indicates the poor heat transfer performance from the hot flue gas to the TEM. A comparison of the isothermal contours on the plate fin (Fig. 8**b**) and the square pin fins (Fig. 8**c-8 l**) suggests that the former has a much lower temperature distribution, reflecting the relatively poor heat transfer by the plate fin. Nevertheless, the hot plate of the TEM temperature with plate fins (Fig. 8**b**) is still much higher than that without fins (Fig. 8**a**). For the TEM with square pin fins, fins' isothermal contours tend to go up with increasing the number of square pin fins. These results are aligned with the observations of Jang et al. [15] where they reported that, under a fixed fin height, the hot side temperature of a TEM increased with increasing the number of fins. Alternatively, along the hot flow direction, the temperatures of the square pin fins are lowered from the upstream to the downstream, say, Fig. 8**l**. This is attributed to the front square pin fins absorbing more heat. As a result, heat received by the rear square pin fins is reduced. This phenomenon has also been highlighted by Borcuch et al. [40] under various types of fins in a hot side heat exchanger.

3.2. Heat transfer rate and TEM performance

Based on the isothermal contours observed in Figs. 7 and 8, the heat transfer characteristic from the hot fluid to the TEM is examined in Fig. 9. A comparison of the heat transfer rate between the TEM without fins and with plate fins reveals that the latter (=85.85 W) is 5.34 folds of the former (=16.08 W). Alternatively, the heat transfer on the hot side of the TEM with 6 × 6 square pin fins is (=81.76 W) 5.08 times that without fins. This arises from the fact that adding fins in the hot channel can not only increase the heat transfer area but also intensify fluid turbulence and local convective heat transfer coefficient, thereby improving the heat transfer efficiency [41].

Li et al. [42] studied plate fins with different geometric dimensions and found that the larger the heat transfer area of the plate fin, the greater the thermal performance. As the number of square pin fins increases, the heat transfer from the hot side of the TEM, the surface area, and the total volume of square pin fins also increase, as shown in Fig. 9. When the number of square pin fins reaches 48, even though the surface area of the square pin fins is lower than that with plate fins (Fig. 9**b**), the heat transfer rate at the hot side of the TEM with square pin fins exceeds that with plate fins (Fig. 9**a**). This is assigned to the higher heat transfer coefficient and lower thermal resistance of the square pin fins when compared with those of plate fins [43,44]. The total volume of the square pin fins stands for its material cost, and this cost rises with increasing the number of square pin fins (Fig. 9**c**). Fig. 9**a** depicts that increasing the number of square pin fins enhances the heat transfer rate; however, once the number of square pin fins is higher than 78, the heat transfer rate is somewhat lowered but the material cost keeps growing, rendering that the optimal number of square pin fins for heat transfer is 78.

The profiles of output power and efficiency of the TEM with different fins installations are demonstrated in Fig. 10. The output power and efficiency of the TEM with plate fins are 4.93 W and 5.74 %, respectively, which are much higher than the TEM without fins (0.16 W and 1.03 %). For the square pin fins, the output power of the TEM is in the

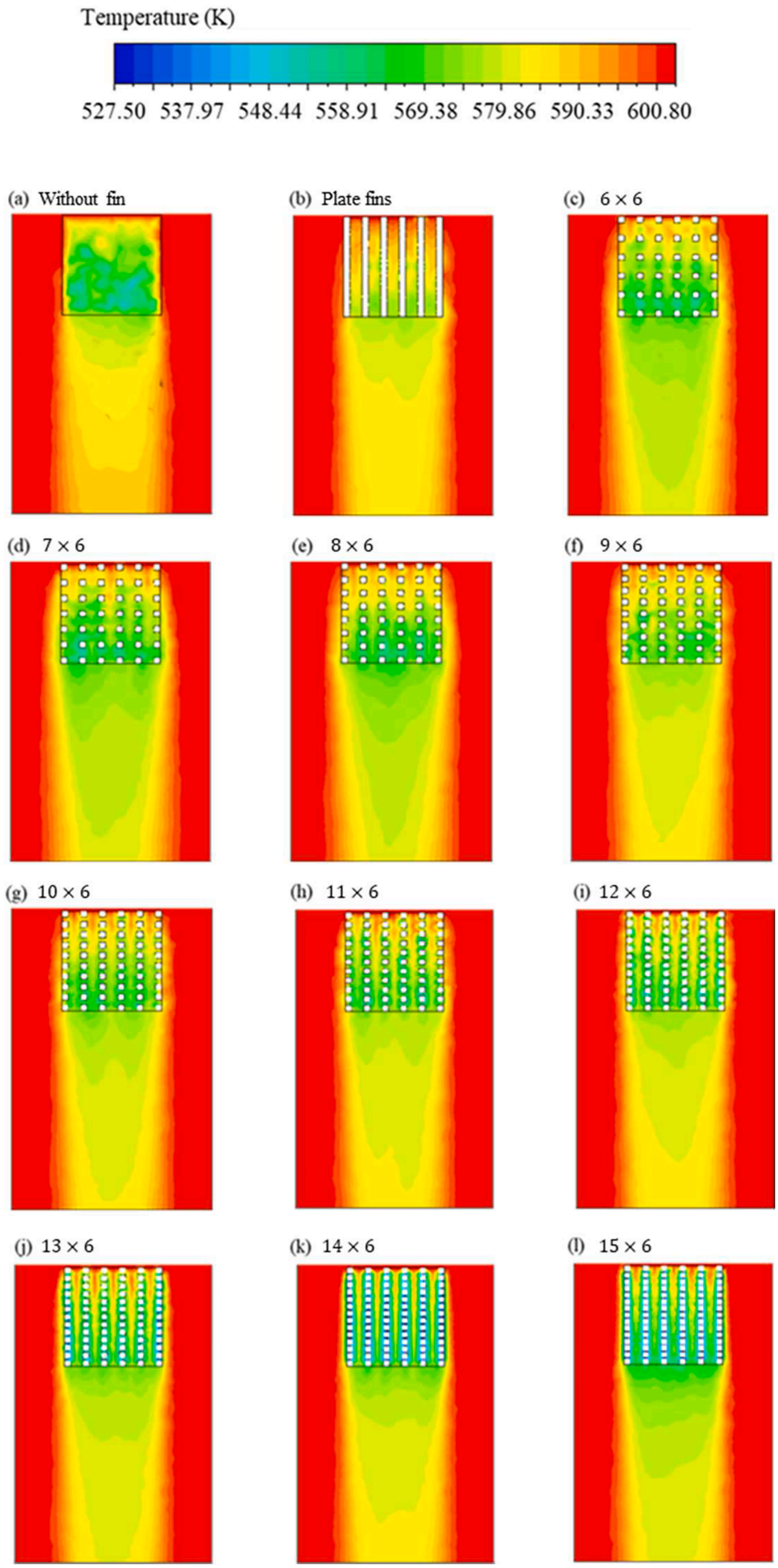

Fig. 7. Isothermal contours of the upper surface of the hot fluid close to the pipe with (a) without fins (b) plate fins (c-l) square pin fins (36–90). ($\dot{m}_h = 0.028\text{kg}\bullet\text{s}^{-1}$ and $T_h = 603.15\text{K}$).

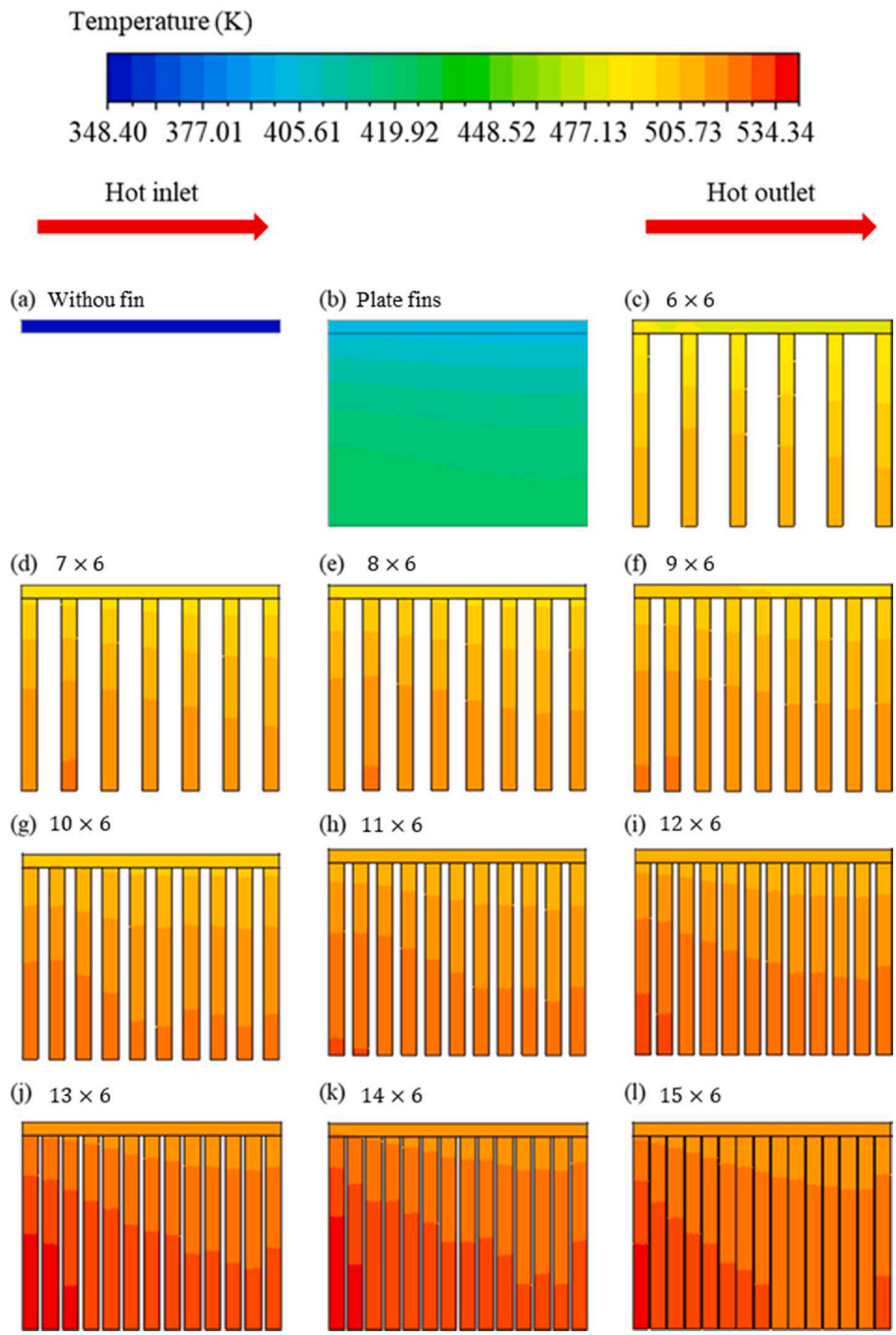

Fig. 8. Isothermal contours of the (a) without fins (b) plate fins (c-I) square pin fins (36–90). ($\dot{m}_h = 0.028\text{kg}\bullet\text{s}^{-1}$ and $T_h = 603.15\text{K}$).

range of 4.45 to 6.12 W, while the efficiency ranges from 5.45 % to 6.42 %. When the number of square pin fins is equal to or exceeds 48, the total output power and efficiency of the TEM are beyond those of the plate fins. The total output power of the system with square pin fins from 36 to 90 is 27.8 to 37.5 times that of the system without fins. Ma et al. [39] studied longitudinal vortex generators (LVGs) with plate fins and used thermoelectric generators to recover waste heat emitted by vehicles. Compared channels with plate fins and smooth channels showed that the total output power increased by 59–153 % from the plate fins. Accordingly, installing fins can increase output power and efficiency significantly, and the present study provides a more obvious improvement. In the present study, the efficiency of the TEM with plate fins is 5.6 times that without fins, and the TEM with square pin fins from 36 to 90 is 5.3 to 6.2 times that without fins (Fig. 10**b**). These results reveal that the influence of fins on output power is by far higher than on efficiency.

It is noteworthy in Fig. 10 that when the number of square pin fins increases from 78 to 84, the output power and efficiency are prone to decline slightly. Again, this is due to the smaller interval smaller between fins, resulting in insufficient heat absorption by the fins. Accordingly, the maximum output power occurs at 78 square pin fins, and this value is higher than that of plate fins by 24.14 %. This phenomenon was also observed by Jang et al. [15]. They studied the effect of different numbers and heights of plate fins on the performance of the TEG; as the number of plate fins increased, the output power of the TEG rose to a certain value and then decreased. The study of Yüncü et al. [45] with different arrays of fins observed the effects of the interval, thickness, height, and the number of fins on the heat transfer rate of a cooling system and compared with the substrate without fins. In the cooling

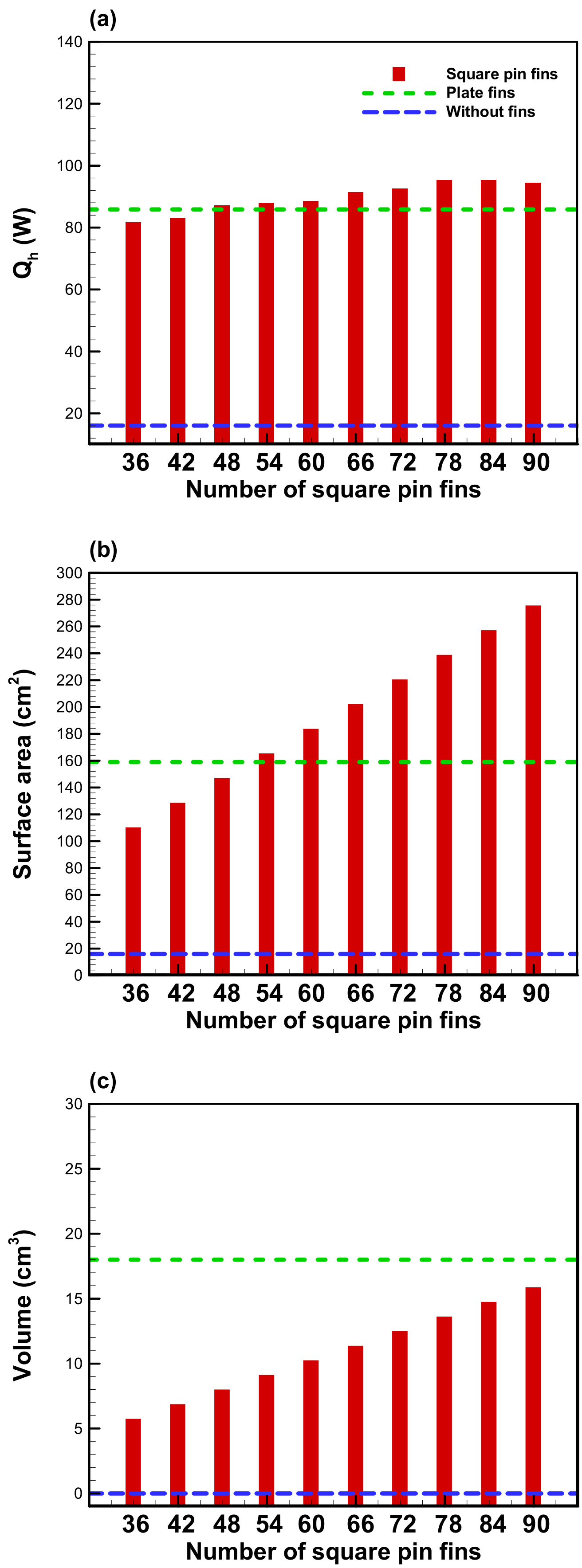

Fig. 9. Comparison of the (a) Q_h, (b) surface area and (c) volume of without fins, plate fins and square pin fins. ($\dot{m}_h = 0.028\text{kg}\bullet\text{s}^{-1}$ and $T_h =$ 603.15K).

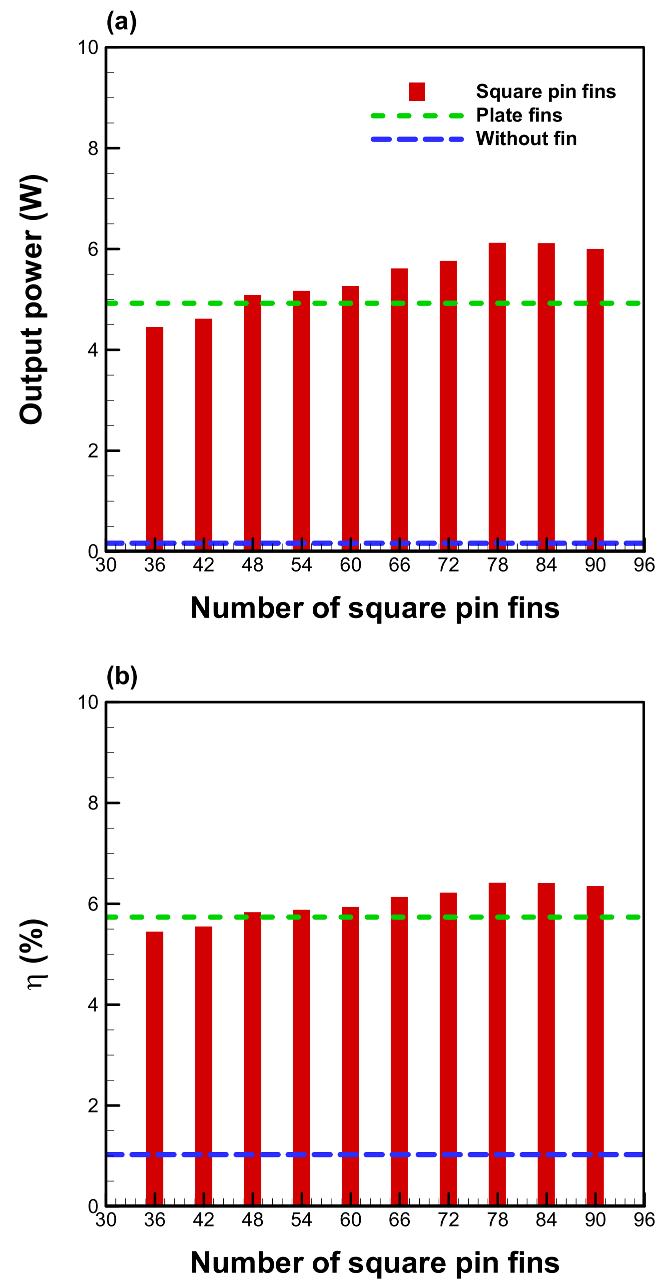

Fig. 10. Comparison of the (a) output power and (b) conversion efficiency of without fins, plate fins and square pin fins. ($\dot{m}_h = 0.028\text{kg}\bullet\text{s}^{-1}$ and $T_h =$ 603.15K).

system with fixed-height fins, as the fin spacing increased, the heat transfer rate reached the maximum value and then decreased. Therefore, the optimal fin spacing was found. The study of Yadav et al. [46] on square microchannel with cylindrical microfins also had similar results, showing that after reaching a maximum value, the heat transfer performance decreased with rising the number of fins. Table 3 shows the maximum output power and efficiency of other studies with various fins along with the average temperature differences between the hot side and cold side of TEMS. The comparison suggests that the design of square pin fins in the present study gives rise to relatively good performance. For example, in the study of Jane et al. [15] with plate fins, the temperature difference was 151 K, and the maximum output power and efficiency were 2.70 W and 3.50 %, respectively, that are lower than the results in this study.

Table 3
Literature reviews of adding fin for thermoelectric generators system.

Type of fins	Working fluid	Maximum power (W)	Maximum efficiency (%)	ΔT (K)	Ref.
Plate fins	HS: exhaust gas CS: water	3.73	1.04	50	[37]
Plate fins	HS: flue gas CS: water	2.70	3.50	151	[15]
Baffler	HS: exhaust flow CS: air, water	12.50	–	64	[57]
Plate fins	HS: waste gas CS: water	3.25	–	202	[58]
Plate fins	HS: waste gas CS: fixed (363.15 K)	1.33	3.23	310	[39]
Plain fins, Offset strip fins, triangular fins	HS: exhaust gas CS: water	44.37	–	343	[59]
Plate fins	HS: exhaust gas CS: water	2.39	–	200	[60]
Plate fins	HS: exhaust gas CS: water	17.39	–	86	[61]
Plate fins	HS: exhaust gas CS: water	13.08	2.58	282	[50]
Plate fins Square pin fins	HS: exhaust gas CS: water	4.93 6.12	5.74 6.42	134 145	This study

3.3. Compromise of heat transfer and material cost

To find the optimal installation of square pin fins, two indexes of Q_r and Q_s are introduced. Q_r is defined as the heat flow rate ratio of square pin fins to plate fins; Q_s is designated as the heat flux ratio (the area is in terms of the surface area of square pin fins or plate fins). The profiles of Q_r and Q_s versus the number of square pin fins are plotted in Fig. 11**a**. It depicts that Q_r is prone to increase with increasing the number of square pin fins. However, Q_s monotonically decreases, showing that the heat flux declines. Meanwhile, the profiles of Q_r and Q_s versus the volume ratio of square pin fins to plate fins are shown in Fig. 11**b**. Based on the predicted data, the curves of Q_r and Q_s can be fitted by two polynomials which are expressed as follows:

$$Q_r = 0.95 - 0.44x + 1.55x^2 - 0.96x^3, R^2 = 0.9742 \tag{21}$$

$$Q_s = 3.24 - 7.63x + 8.34x^2 - 3.37x^3, R^2 = 0.9990 \tag{22}$$

where x is the volume ratio of square pin fins to plate fins. On account of the high coefficients of determination ($R^2 \geq 0.9742$), it shows the excellent fitting of the two curves. Chen et al. [47] studied the optimized heat sink under a fixed volume of a TEG through a compromise programming method, and a compromise point was obtained from the performance of a TEG. In comparison to the basic conditions, the output power density of the TEG was enhanced by 88.70 % at the compromise point, while the efficiency of the heat sink was only reduced by 20.93 %. Physically, while the amount of required material for fins (x) increases, the heat transfer also goes up. In other words, better heat transfer performance acquires more fins, but the material cost rises. Therefore, it is necessary to find a compromise between heat transfer performance and material cost, which can be obtained from the intersection between the two curves shown in Fig. 11**b**. The value of the compromise point is 0.54 where the closest point of the designed square pin fins is 0.5625 which corresponds to 54 square pin fins. Although this number does not lead to the highest output power, in the consideration of cost, the required material for 54 square pin fins is only 0.56 times that of plate fins. Accordingly, the design with 54 square pin fins is adopted for the following predictions.

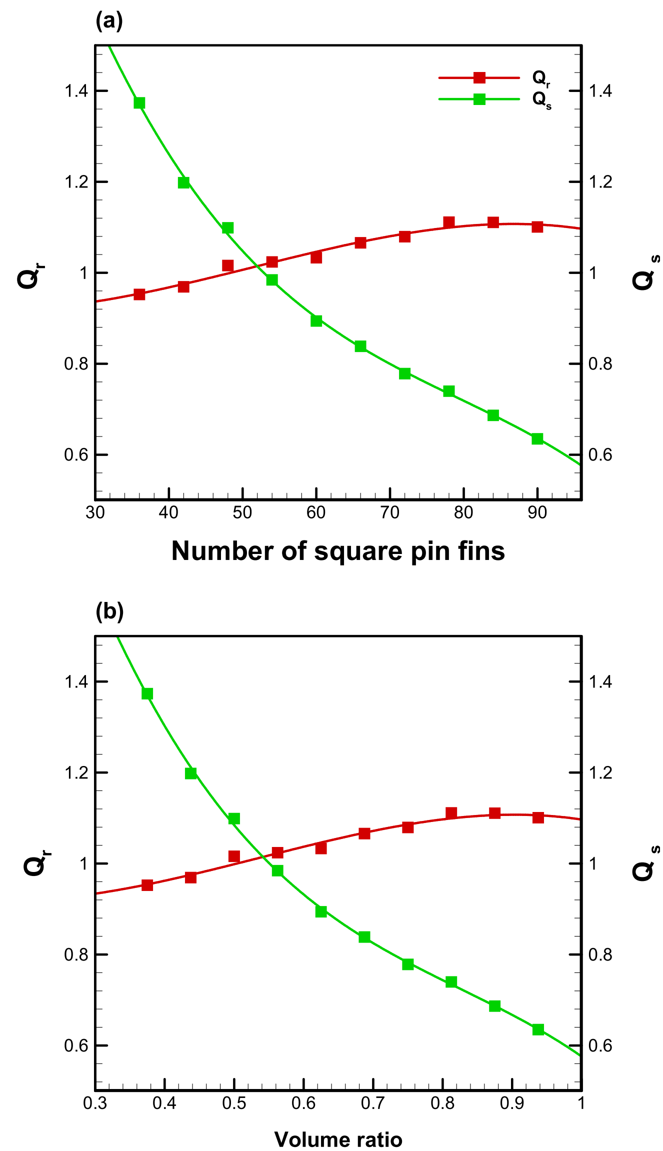

Fig. 11. The Q_r and Q_s under (a) different numbers of square pin fins and (b) volume ratio. ($\dot{m}_h = 0.028\text{kg}\cdot\text{s}^{-1}$ and $T_h = 603.15\text{K}$).

3.4. Effect of different temperatures under the various mass flow rates

Normally, the temperature range of automotive exhaust is between 473.15 K and 773.15 K [34,35,48], depending on the weight, speed, and torque of the automotive engine and the time of the automotive used. Therefore, five different exhaust temperatures of 503.15, 553.15, 603.15, 653.15, and 703.15 K are taken into account to evaluate the influence of the hot flue gas temperature on the heat transfer and performance of the TEM. Meanwhile, five different mass flow rates of the exhaust of 0.028, 0.037, 0.043, 0.046, and 0.05 kg·s^{-1} are regarded [49]. Fig. 12 shows the heat transfer rate profiles at the hot side (Q_h) and the average temperature difference (ΔT_{ave}) between the two sides of the TEM at different mass flow rates and temperatures. It is not surprising that an increase in the temperature or mass flow rate raises both Q_h and ΔT_{ave}. As a whole, the impact of varying the exhaust temperature is greater than altering the mass flow rate on Q_h and ΔT_{ave}. It is also noted that when the mass flow rate increases from 0.046 to to 0.05 kg•s^{-1}, Q_h and ΔT_{ave} are only raised by less than 10 W and 20 K, respectively, implying that the influence of increasing mass flow rate on Q_h and ΔT_{ave} plays an insignificant role as long as the mass flow rate is higher than a certain value.

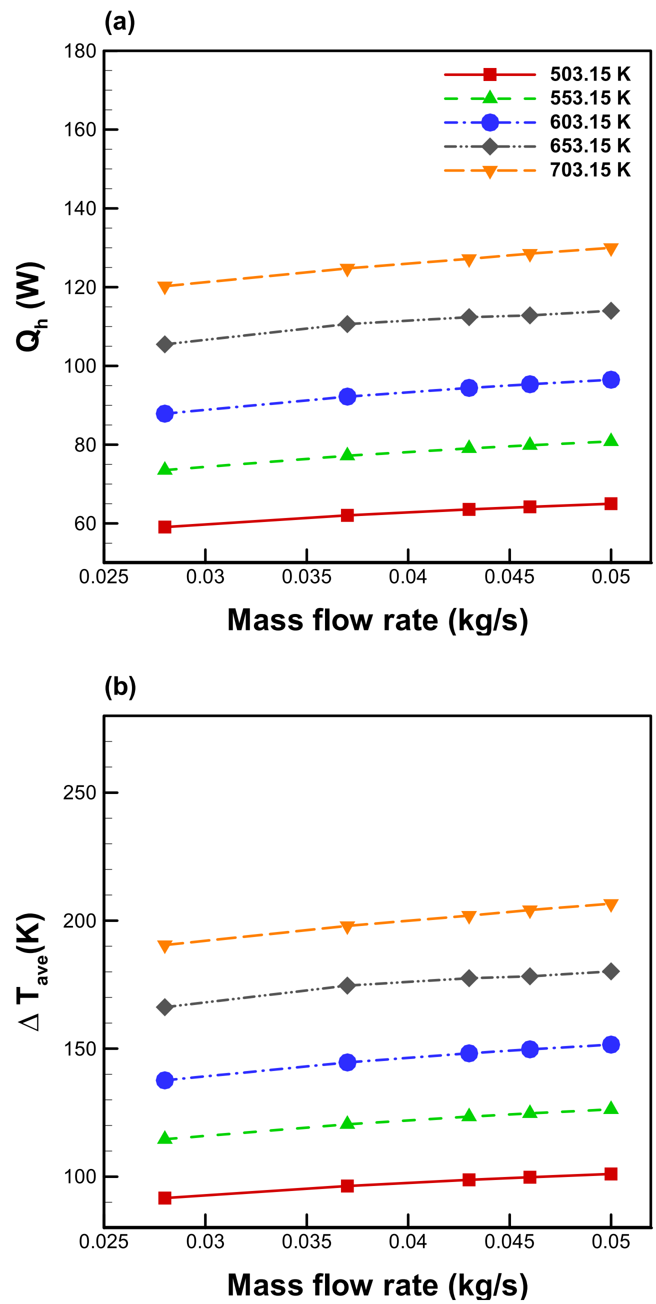

Fig. 12. Comparison of the (a) heat transfer and (b) average temperature difference of the TEM under different mass flow rates and different temperature conditions. (The number of square pin fins are 54).

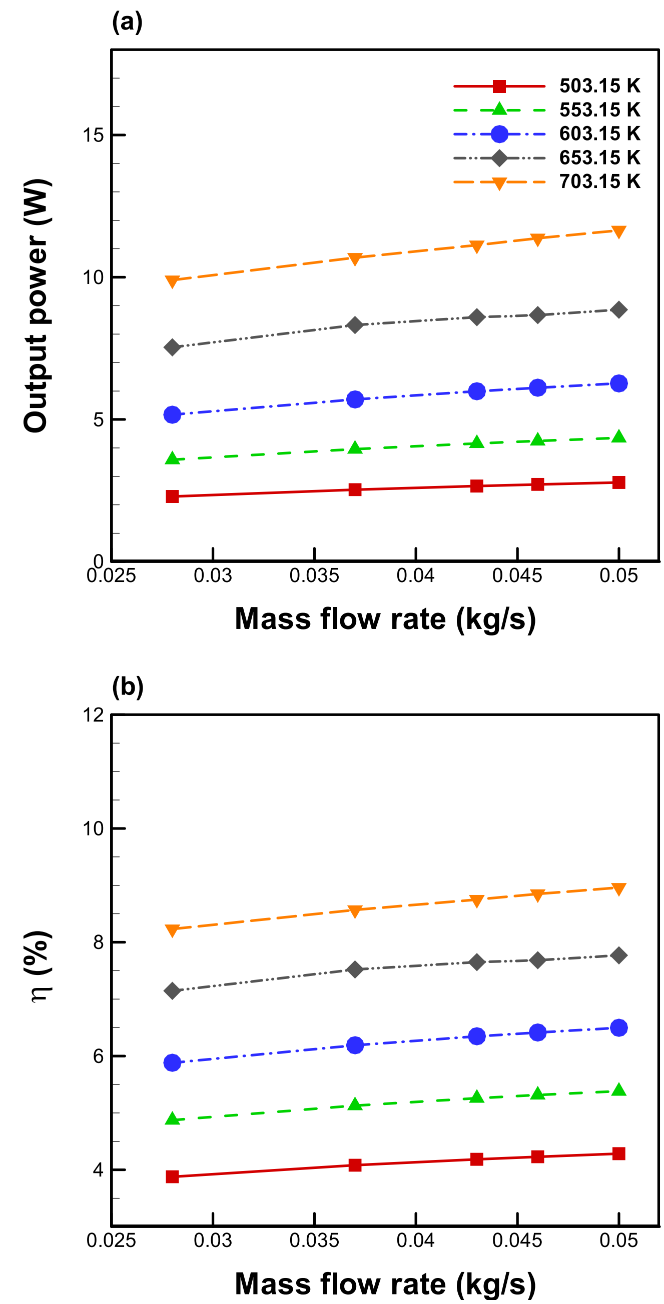

Fig. 13. Comparison of the (a) output power and (b) conversion efficiency under different mass flow rates and different temperature conditions. (The number of square pin fins are 54).

The output power and the conversion efficiency of the TEM are displayed in Fig. 13. Similar to the trends observed in Fig. 12, intensifying waste heat temperature markedly facilitates the output power and efficiency [50]. For instance, for the mass flow rate of 0.028 g·s^{-1}, when the hot fluid temperature increases from 503.15 K to 703.15 K, the output power and efficiency increase from 2.3 W to 9.9 W and from 3.9 % to 8.2 %, respectively. Zhou et al. [35] studied a new structure, which was a cylindrical shell with plate fins to recover vehicle waste heat, and discussed the output power of a TEG at different inlet temperatures. Their results showed that when the inlet temperature went up 100 K, the output power of the TEG rose more than 40 %. It follows that increasing waste heat temperature can effectively increase the output power and efficiency. It should be pointed out that when the mass flow is increased by twice, the output power and efficiency only increase by less than 2 W and 1 %, respectively, regardless of the waste heat temperature. Wang et al. [51] studied a TEG device in which the heat source was automobile exhaust, and explored the influence of different mass flow rates on output power and efficiency. They discovered that when the mass flow rate increased from 10 g·s^{-1} to 30 g·s^{-1}, the output power only increased to a small extent. This is because the mass flow rate of the exhaust was too high, causing insufficient waste heat absorption by TEG.

3.5. Pressure drop and net output power

The pressure drop (the pressure difference between the inlet and outlet of the hot channel, ΔP) profiles under various fin installations are shown in Fig. 14**a**. The pressure drop of the hot channel without fins is 5.15 Pa, and it is 11.33 Pa for the channel with the plate fins. For the

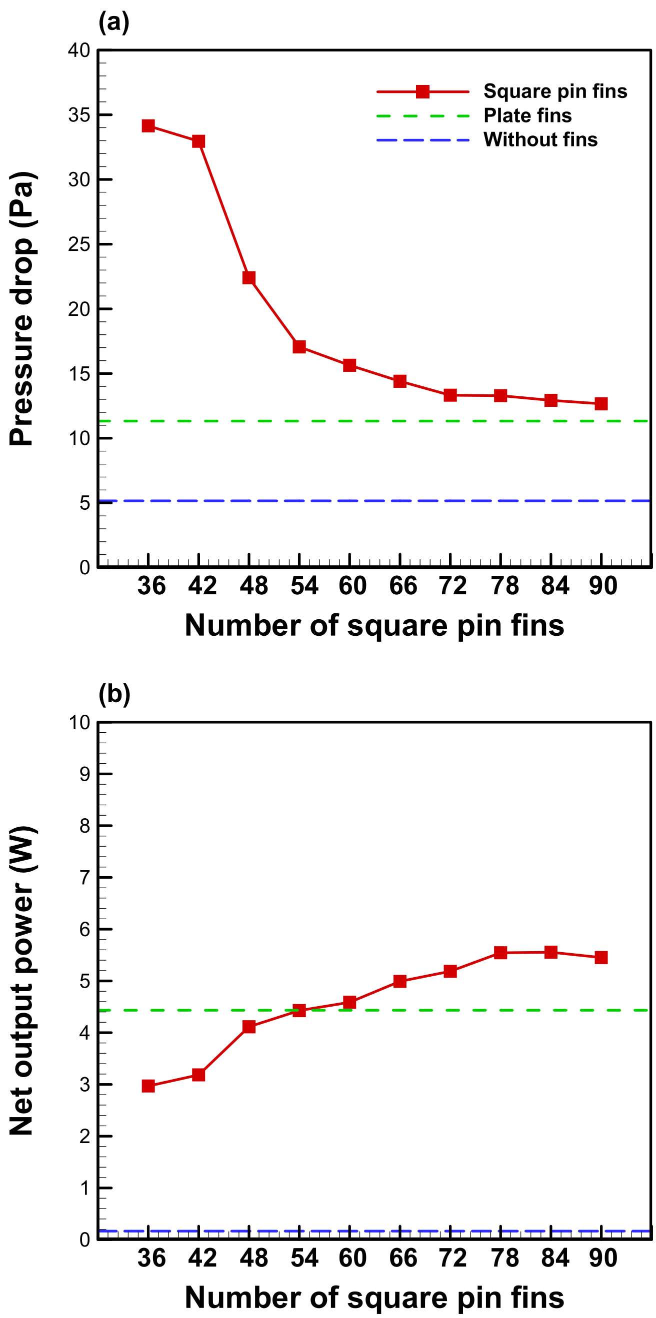

Fig. 14. Comparison of the (a) pressure drop and (b) net output power of systems without fins, plate fins and different numbers of square pin fins. ($\dot{m}_h = 0.028\text{kg}\bullet\text{s}^{-1}$ and $T_h = 603.15\text{K}$).

channel with square pin fins, its pressure drop is always higher than that with plat fins. This is ascribed to more pronounced flow separation around the square pin fins, which leads to larger energy dissipation and thereby pressure drop than plate fins [52]. When the number of square pin fins increases from 36 to 90, the pressure drop decays from 34.15 Pa to 12.66 Pa which is close to that with plate fins. This is attributed to more square pin fins making the geometry approach the plate fins.

The pumping power (P_{pump}) is calculated as the following [39]:

$$P_{pump} = \dot{V}\Delta P \tag{23}$$

where $\dot{V}$ is the volumetric flow rate of the hot fluid. Based on the output power of the TEM (P_{out}) and the pumping power (P_{pump}), the net output power (P_{net}) is calculated as [40]:

$$P_{net} = P_{out} - P_{pump} \tag{24}$$

where P_{out} is the output power of the TEM. The profile of P_{out} with the number of square pin fins are shown in Fig. 10**a**, and the net output power profile versus the number of square pin fins is shown in Fig. 14**b**. The net output power values of the TEM with plate fins, square pin fins, and without fins are 4.43 W, 2.97–5.45 W, and 0.16 W, respectively. This implies that the net output power values of the TEM with plate fins and square pin fins are 27.69 and 18.56–34.06 folds that without fins. Congshun et al. [53] reported that the heat transfer performance of pin fins was better than that of plate fins, and the pressure drop only increased 7.8 %. In the present study, when the number of square pin fins is lower than 54, the system's net output power is lower than that of plate fins. Consequently, the application with 36–48 square pin fins can be disregarded. For 54 square pin fins, the net output power of the system is almost equivalent to that with plate fins, but it only needs 0.56 times material cost of the plate fins. The net output power reaches a maximum value at 78 square pin fins.

The pressure drop and net output power profiles versus the mass flow rate of the hot fluid are shown in Fig. 15**a**. As the mass flow rate increases, the pressure drop also goes up, which means that more pumping power is required [50,54–56]. So Fig. 15**b** depicts that the net output power decreases with increasing mass flow rates and decreasing hot fluid temperatures. It is noteworthy that at the hot fluid temperatures of 503.15 and 552.15 K, the values of the net output power are even negative at certain mass flow rates, showing unsuitable operating conditions. According to the above results, increasing mass flow rate can enhance the TEM's output power, but additional pumping power will reduce the net output power of the system. For automotive exhaust with a higher mass flow rate, a high flue gas temperature is a countermeasure to obtain higher net output power.

4. Conclusions

The heat transfer and output power characteristics of a thermoelectric module (TEM) with/without fin installation have been investigated in this study using a three-dimensional fully numerical simulation method. The TEM is between a hot channel and a cold channel in which the flows are turbulent and the automotive exhaust is used as the waste heat source. The predictions suggest that installing either plate fins or square pin fins can markedly intensify the heat transfer rates, output power, and efficiency of the TEM, especially for the output power improvement. When the number of square pin fins reaches 48, the heat transfer rate at the hot side of the TEM with pin fins exceeds that with plate fins, and the maximum heat transfer rate develops at the number of square pin fins of 78. However, a higher number of square pin fins leads to a higher material cost. Therefore, this study develops a compromise method to find a compromise point between the heat transfer rate and the material cost, which occurs at the number of square pin fins of 54. This leads to the required material being only 0.56 times that of plate fins. The influences of the exhaust temperature and its mass flow rate on the performance of the TEM are also regarded. The results indicate that the performance is significantly affected by the temperature, whereas the mass flow rate plays a minor role. Finally, the pressure drop is taken into account to evaluate the net output power of the TEM system. Though installing more square pin fins gives rise to a higher pressure drop, the net output power of the TEM increases with increasing the number of square pin fins and the highest value occurs at 78. Overall, the present study has provided practical insights into the design of square pin fins in a TEM system for intensifying its performance

CRediT authorship contribution statement

Wei-Hsin Chen: Conceptualization, Formal analysis, Funding acquisition, Investigation, Project administration, Resources, Software,

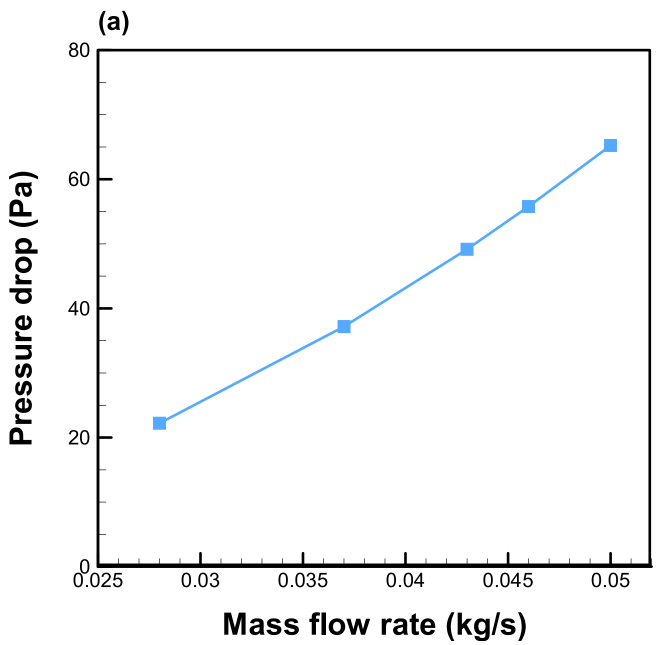

Fig. 15. Comparison of the (a) pressure drop and (b) net output power under different mass flow rates and different temperature conditions. (The number of square pin fins are 54).

Supervision. **Chi-Ming Wang:** Methodology, Validation, Formal analysis, Investigation, Visualization, Writing – original draft. **Lip Huat Saw:** Investigation. **Anh Tuan Hoang:** Investigation. **Argel A. Bandala:** Investigation.

Declaration of Competing Interest

The authors declare that they have no known competing financial interests or personal relationships that could have appeared to influence the work reported in this paper.

Acknowledgments

The authors acknowledge financial support from the Ministry of Science and Technology Taiwan, R.O.C., under the grant numbers MOST 110-2221-E-006-145-MY3 and MOST 110-2622-E-006-001-CC1 for this research.

References

[1] Su Z, Zhang M, Xu P, Zhao Z, Wang Z, Huang H, et al. Opportunities and strategies for multigrade waste heat utilization in various industries: A recent review. Energy Convers Manage 2021;229:113769. https://doi.org/10.1016/j.enconman.2020.113769.
[2] Tang S, Wang C, Liu X, Su G, Tian W, Qiu S, et al. Experimental investigation of a novel heat pipe thermoelectric generator for waste heat recovery and electricity generation. Int J Energy Res 2020;44(9):7450–63.
[3] Pourkiaei SM, Ahmadi MH, Sadeghzadeh M, Moosavi S, Pourfayaz F, Chen L, et al. Thermoelectric cooler and thermoelectric generator devices: A review of present and potential applications, modeling and materials. Energy. 2019;186:115849. https://doi.org/10.1016/j.energy.2019.07.179.
[4] Champier D. Thermoelectric generators: A review of applications. Energy Convers Manage 2017;140:167–81.
[5] Shen Z-G, Tian L-L, Liu X. Automotive exhaust thermoelectric generators: Current status, challenges and future prospects. Energy Convers Manage 2019;195:1138–73.
[6] Sahin AZ, Ismaila KG, Yilbas BS, Al-Sharafi A. A review on the performance of photovoltaic/thermoelectric hybrid generators. Int J Energy Res 2020;44(5):3365–94.
[7] Li P, Ai X, Zhang Q, Gu S, Wang L, Jiang W. Enhanced thermoelectric performance of hydrothermally synthesized polycrystalline Te-doped SnSe. Chin Chem Lett 2021;32(2):811–5.
[8] Karana DR, Sahoo RR. Thermohydraulic performance of a new internal twisted ribs automobile exhaust heat exchanger for waste heat recovery applications. Int J Energy Res 2020;44(14):11417–33.
[9] El-Sheikh HA, Gurimella SV. Enhancement of air jet impingement heat transfer using pin-fin heat sinks. IEEE Trans Compon Packag Technol 2000;23(2):300–8.
[10] T S, D SK. Heat transfer study on different surface textured pin fin heat sink. Int Commun Heat Mass Transfer 2020;119:104902. https://doi.org/10.1016/j.icheatmasstransfer.2020.104902.
[11] Haghighi SS, Goshayeshi HR, Safaei MR. Natural convection heat transfer enhancement in new designs of plate-fin based heat sinks. Int J Heat Mass Transf 2018;125:640–7.
[12] Maji A, Choubey G. Improvement of heat transfer through fins: A brief review of recent developments. Heat Transfer. 2020;49(3):1658–85.
[13] Jang D, Yu S-H, Lee K-S. Multidisciplinary optimization of a pin-fin radial heat sink for LED lighting applications. Int J Heat Mass Transf 2012;55(4):515–21.
[14] Jonsson H, Moshfegh B. Modeling of the thermal and hydraulic performance of plate fin, strip fin, and pin fin heat sinks-influence of flow bypass. IEEE Trans Compon Packag Technol 2001;24(2):142–9.
[15] Jang J-Y, Tsai Y-C, Wu C-W. A study of 3-D numerical simulation and comparison with experimental results on turbulent flow of venting flue gas using thermoelectric generator modules and plate fin heat sink. Energy. 2013;53:270–81.
[16] Rezania A, Rosendahl LA. A comparison of micro-structured flat-plate and cross-cut heat sinks for thermoelectric generation application. Energy Convers Manage 2015;101:730–7.
[17] Şara ON. Performance analysis of rectangular ducts with staggered square pin fins. Energy Convers Manage 2003;44(11):1787–803.
[18] Peltonen P, Saari K, Kukko K, Vuorinen V, Partanen J. Large-Eddy Simulation of local heat transfer in plate and pin fin heat exchangers confined in a pipe flow. Int J Heat Mass Transf 2019;134:641–55.
[19] Yang K-S, Chu W-H, Chen I-Y, Wang C-C. A comparative study of the airside performance of heat sinks having pin fin configurations. Int J Heat Mass Transf 2007;50(23):4661–7.
[20] Chen M, Rosendahl LA, Condra T. A three-dimensional numerical model of thermoelectric generators in fluid power systems. Int J Heat Mass Transf 2011;54(1-3):345–55.
[21] Seo YM, Ha MY, Park SH, Lee GH, Kim YS, Park YG. A numerical study on the performance of the thermoelectric module with different heat sink shapes. Appl Therm Eng 2018;128:1082–94.
[22] Bejjam RB, Dabot M, Wondatir T, Negash S. Performance evaluation of thermoelectric generator using CFD. Mater Today: Proc 2021;47:2498–504.
[23] Luo D, Wang R, Yan Y, Yu W, Zhou W. Transient numerical modelling of a thermoelectric generator system used for automotive exhaust waste heat recovery. Appl Energy 2021;297:117151. https://doi.org/10.1016/j.apenergy.2021.117151.
[24] Chen W-H, Lin Y-X, Chiou Y-B, Lin Y-L, Wang X-D. A computational fluid dynamics (CFD) approach of thermoelectric generator (TEG) for power generation. Appl Therm Eng 2020;173:115203. https://doi.org/10.1016/j.applthermaleng.2020.115203.
[25] Kim TY, Lee S, Lee J. Fabrication of thermoelectric modules and heat transfer analysis on internal plate fin structures of a thermoelectric generator. Energy Convers Manage 2016;124:470–9.
[26] Ahsan M. Numerical analysis of friction factor for a fully developed turbulent flow using k–ε turbulence model with enhanced wall treatment. Beni-Suef University Journal of Basic and Applied Sciences. 2014;3(4):269–77.
[27] Rolander N, Rambo J, Joshi Y, Allen JK, Mistree F. An Approach to Robust Design of Turbulent Convective Systems. J Mech Des 2006;128(4):844–55.

[28] Chen W-H, Lin Y-X, Wang X-D, Lin Y-L. A comprehensive analysis of the performance of thermoelectric generators with constant and variable properties. Appl Energy 2019;241:11–24.
[29] Amini Z, Ilham Z, Ong HC, Mazaheri H, Chen W-H. State of the art and prospective of lipase-catalyzed transesterification reaction for biodiesel production. Energy Convers Manage 2017;141:339–53.
[30] Yan Y, Malen JA. Periodic heating amplifies the efficiency of thermoelectric energy conversion. Energy Environ Sci 2013;6(4):1267–73.
[31] Chen W-H, Wu P-H, Wang X-D, Lin Y-L. Power output and efficiency of a thermoelectric generator under temperature control. Energy Convers Manage 2016;127:404–15.
[32] Wang Y, Shi Y, Mei D, Chen Z. Wearable thermoelectric generator to harvest body heat for powering a miniaturized accelerometer. Appl Energy 2018;215:690–8.
[33] Selimefendigil F, Öztop HF, Özgul R. Turbulent forced convection of nanofluid in an elliptic cross-sectional pipe. Int Commun Heat Mass Transfer 2019;109:104384. https://doi.org/10.1016/j.icheatmasstransfer.2019.104384.
[34] Liu C, Deng YD, Wang XY, Liu X, Wang YP, Su CQ. Multi-objective optimization of heat exchanger in an automotive exhaust thermoelectric generator. Appl Therm Eng 2016;108:916–26.
[35] Zhou M, He Y, Chen Y. A heat transfer numerical model for thermoelectric generator with cylindrical shell and straight fins under steady-state conditions. Appl Therm Eng 2014;68(1-2):80–91.
[36] Wang Y, Li S, Xie Xu, Deng Y, Liu X, Su C. Performance evaluation of an automotive thermoelectric generator with inserted fins or dimpled-surface hot heat exchanger. Appl Energy 2018;218:391–401.
[37] Wang Y, Li S, Zhang Y, Yang X, Deng Y, Su C. The influence of inner topology of exhaust heat exchanger and thermoelectric module distribution on the performance of automotive thermoelectric generator. Energy Convers Manage 2016;126:266–77.
[38] Wang Y, Wu C, Tang Z, Yang X, Deng Y, Su C. Optimization of fin distribution to improve the temperature uniformity of a heat exchanger in a thermoelectric generator. J Electron Mater 2015;44(6):1724–32.
[39] Ma T, Lu X, Pandit J, Ekkad SV, Huxtable ST, Deshpande S, et al. Numerical study on thermoelectric–hydraulic performance of a thermoelectric power generator with a plate-fin heat exchanger with longitudinal vortex generators. Appl Energy 2017;185:1343–54.
[40] Borcuch M, Musiał M, Gumuła S, Sztekler K, Wojciechowski K. Analysis of the fins geometry of a hot-side heat exchanger on the performance parameters of a thermoelectric generation system. Appl Therm Eng 2017;127:1355–63.
[41] Guo K, Zhang N, Smith R. Design optimisation of multi-stream plate fin heat exchangers with multiple fin types. Appl Therm Eng 2018;131:30–40.
[42] Li H-Y, Chao S-M. Measurement of performance of plate-fin heat sinks with cross flow cooling. Int J Heat Mass Transf 2009;52(13):2949–55.
[43] Micheli L, Reddy KS, Mallick TK. Experimental comparison of micro-scaled plate-fins and pin-fins under natural convection. Int Commun Heat Mass Transfer 2016; 75:59–66.
[44] Kim D-K, Kim SJ, Bae J-K. Comparison of thermal performances of plate-fin and pin-fin heat sinks subject to an impinging flow. Int J Heat Mass Transf 2009;52 (15):3510–7.
[45] Yüncü H, Anbar G. An experimental investigation on performance of rectangular fins on a horizontal base in free convection heat transfer. Heat Mass Transf 1998;33 (5-6):507–14.
[46] Yadav V, Baghel K, Kumar R, Kadam ST. Numerical investigation of heat transfer in extended surface microchannels. Int J Heat Mass Transf 2016;93:612–22.
[47] Wang C-C, Hung C-I, Chen W-H. Design of heat sink for improving the performance of thermoelectric generator using two-stage optimization. Energy. 2012;39(1): 236–45.
[48] Espinosa N, Lazard M, Aixala L, Scherrer H. Modeling a thermoelectric generator applied to diesel automotive heat recovery. J Electron Mater 2010;39(9):1446–55.
[49] Yu G, Shu G, Tian H, Wei H, Liu L. Simulation and thermodynamic analysis of a bottoming Organic Rankine Cycle (ORC) of diesel engine (DE). Energy. 2013;51: 281–90.
[50] Cao Q, Luan W, Wang T. Performance enhancement of heat pipes assisted thermoelectric generator for automobile exhaust heat recovery. Appl Therm Eng 2018;130:1472–9.
[51] Wang Y, Dai C, Wang S. Theoretical analysis of a thermoelectric generator using exhaust gas of vehicles as heat source. Appl Energy 2013;112:1171–80.
[52] Zhou F, Catton I. Numerical evaluation of flow and heat transfer in plate-pin fin heat sinks with various pin cross-sections. Numerical Heat Transfer, Part A: Applications. 2011;60(2):107–28.
[53] Congshun W, Youmin Y, Simon T, Tianhong C, North MT. Microfabrication of short pin fins on heat sink surfaces to augment heat transfer performance. Conference Microfabrication of short pin fins on heat sink surfaces to augment heat transfer performance. p. 944-50.
[54] Niu X, Yu J, Wang S. Experimental study on low-temperature waste heat thermoelectric generator. J Power Sources 2009;188(2):621–6.
[55] Kim TY, Kwak J, Kim B-W. Application of compact thermoelectric generator to hybrid electric vehicle engine operating under real vehicle operating conditions. Energy Convers Manage 2019;201:112150. https://doi.org/10.1016/j.enconman.2019.112150.
[56] Lu H, Wu T, Bai S, Xu K, Huang Y, Gao W, et al. Experiment on thermal uniformity and pressure drop of exhaust heat exchanger for automotive thermoelectric generator. Energy. 2013;54:372–7.
[57] Du Q, Diao H, Niu Z, Zhang G, Shu G, Jiao K. Effect of cooling design on the characteristics and performance of thermoelectric generator used for internal combustion engine. Energy Convers Manage 2015;101:9–18.
[58] Wan QiuShi, Liu X, Gu B, Bai WanRong, Su ChuQi, Deng YaDong. Thermal and acoustic performance of an integrated automotive thermoelectric generation system. Appl Therm Eng 2019;158:113802. https://doi.org/10.1016/j.applthermaleng.2019.113802.
[59] Marvão A, Coelho PJ, Rodrigues HC. Optimization of a thermoelectric generator for heavy-duty vehicles. Energy Convers Manage 2019;179:178–91.
[60] Luo D, Wang R, Yu W, Zhou W. A numerical study on the performance of a converging thermoelectric generator system used for waste heat recovery. Appl Energy 2020;270:115181. https://doi.org/10.1016/j.apenergy.2020.115181.
[61] Stobart R, Wijewardane MA, Yang Z. Comprehensive analysis of thermoelectric generation systems for automotive applications. Appl Therm Eng 2017;112: 1433–44.